

01 Jan 1982

Electron Density Measurements In A Laser Induced Na Plasma

D. J. Krebs

Laird D. Schearer

Missouri University of Science and Technology

Follow this and additional works at: https://scholarsmine.mst.edu/phys_facwork

 Part of the [Physics Commons](#)

Recommended Citation

D. J. Krebs and L. D. Schearer, "Electron Density Measurements In A Laser Induced Na Plasma," *The Journal of Chemical Physics*, vol. 76, no. 6, pp. 2925 - 2930, American Institute of Physics, Jan 1982. The definitive version is available at <https://doi.org/10.1063/1.443375>

This Article - Journal is brought to you for free and open access by Scholars' Mine. It has been accepted for inclusion in Physics Faculty Research & Creative Works by an authorized administrator of Scholars' Mine. This work is protected by U. S. Copyright Law. Unauthorized use including reproduction for redistribution requires the permission of the copyright holder. For more information, please contact scholarsmine@mst.edu.

RESEARCH ARTICLE | MARCH 15 1982

Electron density measurements in a laser induced Na plasma

D. J. Krebs; L. D. Schearer



J. Chem. Phys. 76, 2925–2930 (1982)

<https://doi.org/10.1063/1.443375>

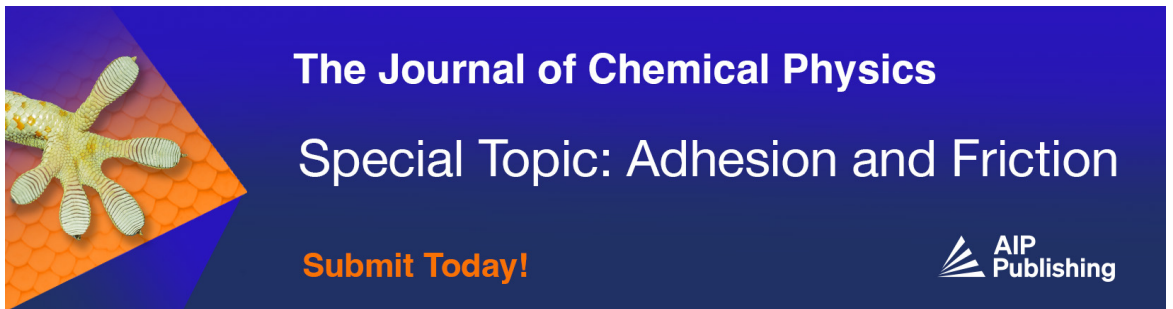


View
Online




Export
Citation

CrossMark



The Journal of Chemical Physics
Special Topic: Adhesion and Friction

Submit Today!



Electron density measurements in a laser induced Na plasma^{a)}

D. J. Krebs^{b)} and L. D. Schearer

University of Missouri-Rolla, Physics Department, Rolla, Missouri 65401
(Received 13 November 1981; accepted 9 December 1981)

The optical emission spectrum of a recombining Na plasma is observed. The shift and broadening of the spectral line emission due to electron collisions is observed. Electron densities on the order of $5 \times 10^{14} \text{ cm}^{-3}$ are calculated from the shift measurements. The results agree well with electron densities obtained in the same system from Saha plots of excited state densities.

I. INTRODUCTION

The electron density in a partially ionized plasma is an important parameter in determining the properties of the gaseous discharge. The current interest in discharge switches, high-power pulsed laser discharges, recombination lasers, and laser induced plasmas has made the determination of the electron density in pulsed systems a necessity.

A variety of techniques exist for the determination of the electron density in a decaying plasma; however, spectral measurements have the advantage that noncontact observations can be made and small volumes sampled within small time intervals.

In this article we report the observation of spectral line shifts and broadening due to electron collisions in a recombining Na plasma. From measurements of the spectral line shifts, the electron density is calculated. The electron density thus obtained is compared with measurements inferred from Saha-Boltzmann plots of the excited Na states in local thermodynamic equilibrium with the electrons. These electron density measurements are also compared with charge removed from the plasma by an applied electric field. The plasma for the experiment described here consists of a line charge of approximately 0.5 mm diameter with electron densities up to 10^{15} cm^{-3} in a cell containing Na (~ 1 Torr) and argon (400 Torr).

II. EXPERIMENTAL APPARATUS

The sodium atoms along with a rare-gas buffer are contained in a stainless steel cross with sapphire windows. The structure is placed in an oven enabling temperatures up to 700 K to be obtained. The Na plasma is produced by laser excitation in a 2 or 3 photon absorption process via the Na($3p$) state. The buffer gas, typically argon at several hundred Torr, is used to eliminate diffusion losses of ions, electrons, and excited atoms from the observation region during the course of the experiment.

Two tunable dye lasers pumped by a single N_2 laser provided 4 ns, 50 μJ pulses at two different frequencies. One laser is tuned to excite one of the 3^2P sodium levels at 589 nm while the second laser can be tuned to

wavelengths between 406 and 564 nm. At 406 nm, the photons have just sufficient energy to photoionize the $3p$ atom. The bandwidth of the lasers is approximately 0.4 Å (FWHM). The two laser beams are passed collinearly through the Na cell and focused at the cell center to ~ 0.3 mm diameter spots. The beam divergences were sufficiently small over the observation region that a very nearly cylindrical column of excited vapor is created. The fluorescence at 90° to the axis of the excited region is observed by an S-20 photomultiplier coupled to a 0.5 m Jarrell-Ash monochromator. The photomultiplier output is analyzed by a PAR 160 boxcar integrator, an SSR 1110 synchronous photon counter, or a Tek 5441 storage oscilloscope with a fast sampling head. A schematic representation of the apparatus is shown in Fig. 1.

III. EXPERIMENTAL OBSERVATIONS

A. Two photon processes

If the second laser is tuned to 406 nm, a sodium atom can be ionized in a two photon, resonant absorption process via the $3p$ state. The laser intensities and pulse widths (50 μJ , 4 ns) do not produce more than a relatively small number ($\sim 10^{12} \text{ cm}^{-3}$) of "seed" electrons via the photoionization process. However, collisional mechanisms involving densely populated excited states and the seed electrons can lead to nearly complete ionization of the Na vapor. This ionization mechanism has been discussed by Lucatorto and McIlrath¹ and Measures and Cardinal,² while energy pooling processes leading to excited state populations in the early afterglow have been discussed by Bearman and Levanthal³ and Allegrini *et al.*⁴ We have examined the kinetics of the energy pooling process and measured rate constants for the formation of the $4d$, $5d$, $6d$, and $6s$ states by collisions between two Na($3p$) atoms.⁵

Optical emission from $nd-3p$ transitions in Na in the afterglow of the laser pulses under the conditions described above is observed. The individual transitions are isolated with a monochromator. A PAR Boxcar Integrator with an aperture of 20 ns is used to temporally scan the wavelength isolated line. Figure 2 shows the fluorescence intensity versus time in the afterglow of the laser pulse for the $5d-3p$ transition. The optical pulse consists of two components: A strong initial pulse of approximately 100 ns duration followed by a rise and slow decay of the fluorescence. The early, fast component is associated with excited state populations pro-

^{a)}Work supported by the Office of Naval Research.

^{b)}Present address: McDonnell Douglas Co., St. Louis, MO 63166.

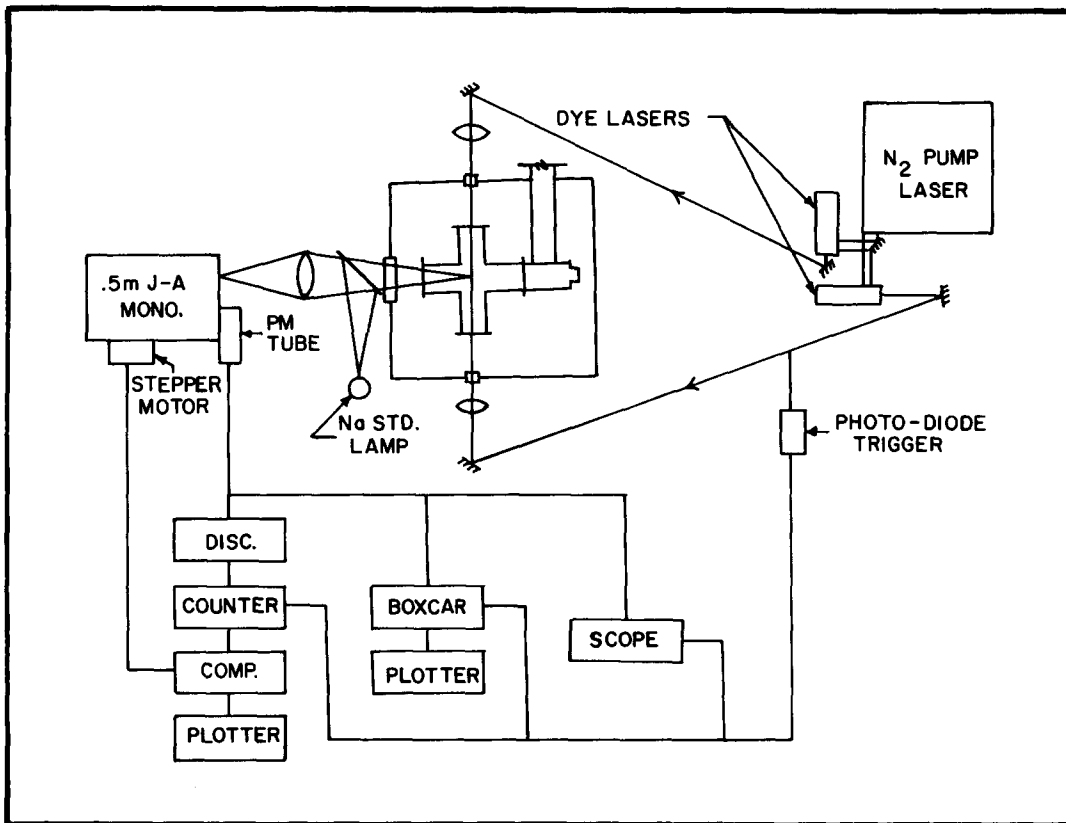


FIG. 1. Schematic of the apparatus.

duced by collisions of two $3p$ atoms. States which are energetically accessible to a Boltzmann distribution of the $3p$ atoms are populated within this first 100 ns following the 589 nm laser pulse. Subsequent to the decay of this fast component a slow component appears and decays on a many microsecond time scale. Emission in this slow component is due to three-body, electron stabilized recombination.

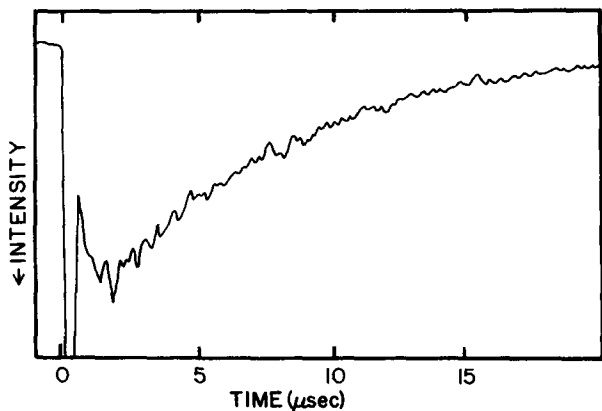


FIG. 2. Fluorescence intensity vs time after laser excitation for the $5d \rightarrow 3p$ transition with both lasers employed. The early fluorescence peak, which is off-scale, is approximately 20 times more intense than the peak of the recombination fluorescence at $t = 2 \mu s$. The second laser is tuned to the ionization threshold of the $3p$ state at 408 nm.

B. Recombination fluorescence

The fluorescence appearing $2 \mu s$ after the laser pulses is due to the recombination process. With the Boxcar Integrator set to a delay of 2 and $0.5 \mu s$ aperture a

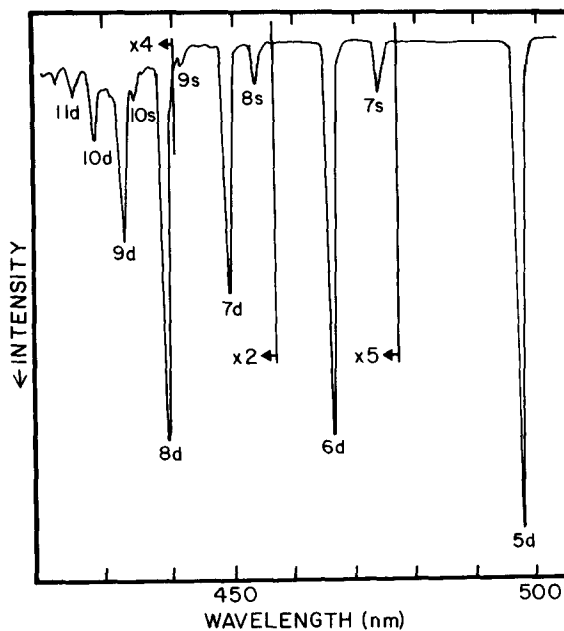


FIG. 3. Recombination fluorescence at $t = 2 \mu s$ vs wavelength. Scan resolution is 0.8 nm (FWHM). The second laser is fixed at 408 nm.

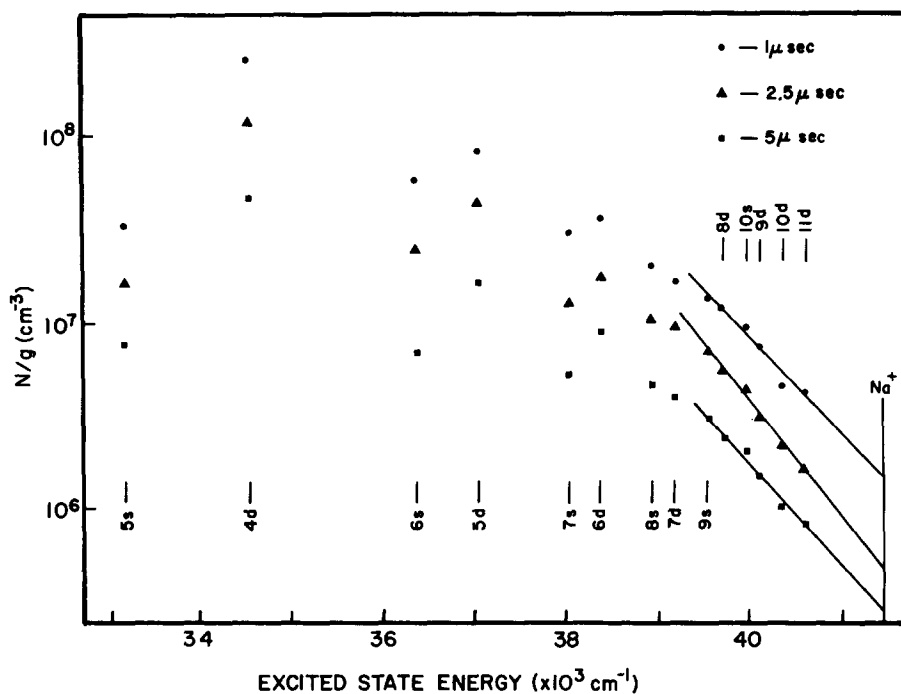


FIG. 4. Saha-Boltzmann plot of excited state densities vs energy level.

monochromator scan of the emission produces the spectrum shown in Fig. 3. The monochromator detection system is calibrated against an absolute standard lamp; thus absolute intensity measurements of the transitions along with radiative decay rates yield absolute excited state densities. Figure 4 is a plot of the absolute excited state density versus the excited state energy. Levels within 0.25 eV of the ionization limit appear to be in local thermodynamic equilibrium with the electrons. Applying the Saha equation

$$n_e^2/N^* = (2g_{10n}/g^*)(2\pi mkT_e)^{3/2} \exp[-(E_{10n} - E^*)/kT_e], \quad (1)$$

one obtains the electron temperature T_e and the electron density n_e . The electron temperature depends only on relative intensities, while the electron density depends on an absolute calibration of the detection system. For the data shown in Fig. 4, we obtain $T_e = 900$ K and $n_e = 3.4 \times 10^{14}$ cm $^{-3}$, 2.5 μ s after the laser pulse. The density measurements are believed accurate within a factor of 3; the electron temperature is accurate to within 10%.

C. Line shift discussion and results

Shifts in the energies of the spectral lines emitted by the Na plasma occur as a result of collisions of the excited Na atoms with both the heavy particles (noble-gas buffer atoms) and/or the plasma electrons. If the collisional events leading to the excited state populations occur in the early afterglow where the electron density is small, any emission line shifts must be associated with collisions of the excited state with the large density of rare-gas buffer atoms. If, on the other hand, the fluorescence from excited states is observed late in the afterglow where the electron density is large, the emission lines are broadened by both collisions with the buffer gas atoms and the large density of elec-

trons. The line shifts due to electron collisions are rather extensively described by Griem,⁷ while Kielkopf and Knollenburg⁸ discuss line shifts of the Na 5d, 6d, and 7d levels, due to collisions with argon atoms. In order to determine the shifts associated with electron collisions it is necessary to separate out the effects due to the buffer gas. At first glance, it would appear that the perturbations due to the buffer gas could be isolated by measuring the shifts as a function of pressure and extrapolating to zero pressure. However, the role of the buffer gas is to confine the excited state populations and ion/electrons to the region defined by the laser beam. At buffer gas densities above approximately 400 Torr the major loss of electron/ion density is via collisional-radiative recombination. At buffer gas densities less than this, a reduction of the electron density by ambipolar diffusion becomes increasingly important. Consequently, varying the buffer gas pressure also changes the electron loss rate. We are thus forced to devise an alternate technique.

1. Pressure shifts: Three photon absorption processes

In Sec. III B, the optical emission from the ionized volume at times greater than 0.5 μ s after the laser pulse was described in terms of collisional-radiative recombination processes. The excited, bound states have lifetimes considerably shorter than the microsecond time scale of Fig. 2. The excited states are either quenched radiatively or collisionally. Thus, any excited state fluorescence observed in the late afterglow must have originated from the recombination of ions and electrons. Since the excited states formed depend only on the details of the recombination process and not on how the ions were originally produced, in the late afterglow the integrated optical emission is proportional to the number of ions formed in the excitation-ionization process.

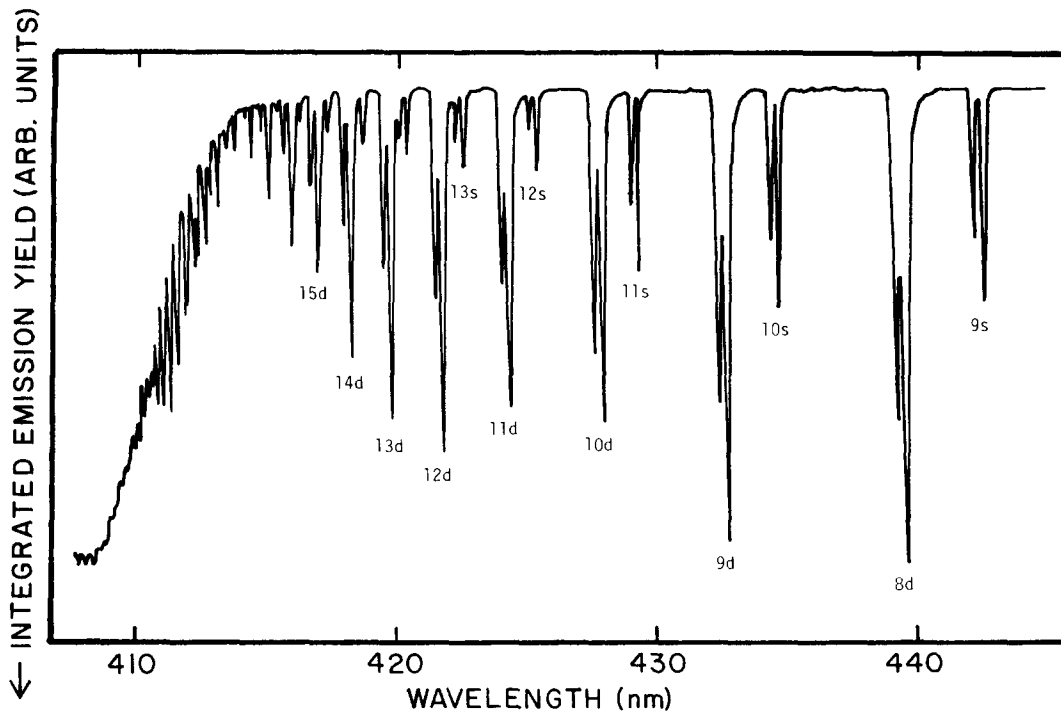


FIG. 5. Scan of fluorescence yield vs the wavelength of the second, ionizing laser. The ionization limit corresponds to a wavelength of 408 nm. Identical spectra are obtained if the ions/electrons are collected directly.

The excitation-ionization process leading to nearly complete ionization can be understood in terms of the electron-seeding model proposed by Measures and Cardinal.² In this model, the presence of a small number of seed electrons produced by photoionization and a densely populated excited state can lead to nearly saturated ionization. The reservoir of excited state atoms is a source of energy which can be transferred to the seed electrons in superelastic collisions. These ener-

getic electrons can now excite and/or ionize the sodium. An excellent description of this process is given in Ref. 2.

If the second (blue) laser is tuned through a $3p \rightarrow nd$ (ns) transition, the number of seed electrons produced is proportional to the transition moment, the laser intensity, and the photoionization cross section of the nd (ns) state.² The seed electron density in turn deter-

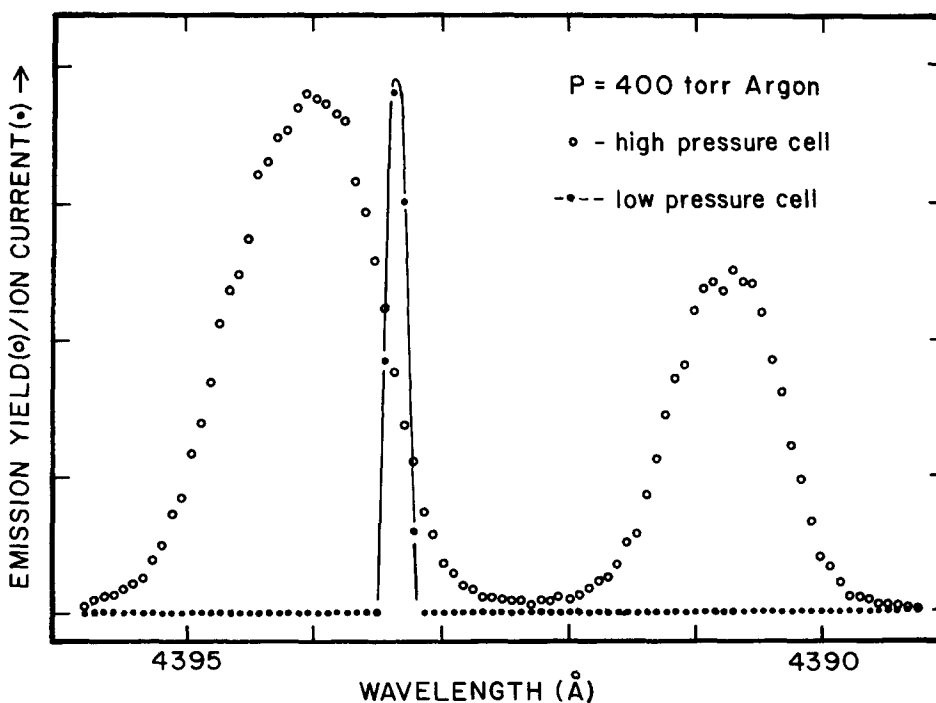


FIG. 6. Fluorescence yield vs laser wavelength for the $3p \rightarrow 8d$ transitions from a scan taken simultaneously in a cell with 400 Torr of argon buffer and a cell with no buffer gas. Two components are present in the high pressure cell due to collisional mixing of the $3^2P_{3/2,1/2}$ levels. Identical spectra are obtained if the ions/electrons are collected directly.

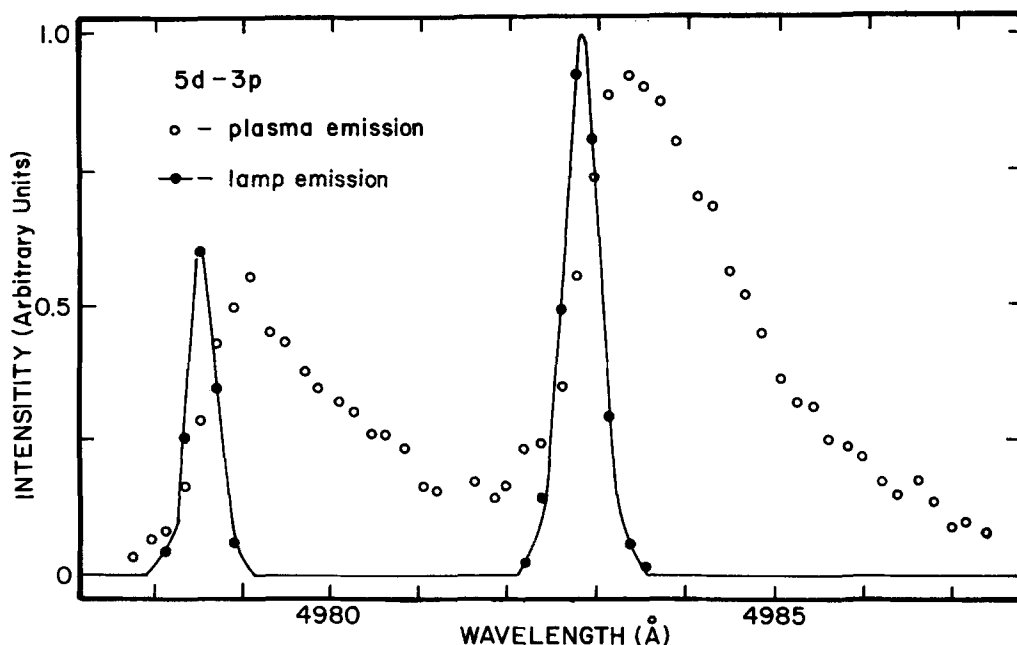


FIG. 7. Simultaneous high resolution scan of plasma emission and lamp emission.

mines the ultimate ion/electron density. If we observe the integrated emission from the interaction zone and scan the frequency of the second laser, we obtain the spectrum shown in Fig. 5. Since the excitation of the nd (ns) excited state takes place only during the 4 ns laser pulse, well before the ion/electron density reaches its peak (see Fig. 2), the shift of the spectral lines as observed while tuning the blue laser through a transition is *due only to the presence of the buffer gas*. A higher resolution tracing as the laser is scanned through the $3p-8d$ transition at 439 nm is shown in Fig. 6. The ion yield is recorded simultaneously in a cell with no buffer gas and a cell with 400 Torr of argon buffer. Two components appear in the high pressure scan representing the $3P_{1/2}$ and $3P_{3/2}$ levels which are collisionally mixed at the high buffer gas pressures. The shift in the emission lines due to the Ar buffer at 400 Torr is then simply determined.

2. Pressure and electron density shifts

The recombination spectrum shown in Fig. 3 is obtained by scanning the monochromator through the respective transitions with the synchronous photon counter set for a delay of $2 \mu\text{s}$ after the laser pulses and with an aperture of $1.0 \mu\text{s}$. This delay corresponds to the maximum electron density, as indicated from Fig. 2. The emission lines are thus shifted (and broadened) both by collisions with electrons and the 400 Torr argon buffer. Figure 7 is a high-resolution monochromator scan of the $6d-3p$ transition under these conditions.

In Fig. 8, we show the shifts for the $3p-5d$, $6d$, and $7d$ transitions obtained by (a) scanning the second dye laser through the transition and (b) scanning the monochromator through the indicated transition. The difference in the shifts between the two curves is then due to the difference in the electron density under the two conditions.

D. Electron density from shift data

Line shifts in Na due to collisions with electrons have been computed theoretically by Griem.⁷ In Fig. 9 the results obtained by Griem are extrapolated to 900 K and an electron density of $6.8 \times 10^{14} \text{ cm}^{-3}$ and shown as circles. A solid line connects the computed shifts to aid the eye. The square points are the experimental shifts we measure by the technique outlined in the preceding sections. A dotted line connects the experimental points. The 900 K electron temperature was derived from our Saha plots as described in Sec. III B. The $6.8 \times 10^{14} \text{ cm}^{-3}$ yields the best fit of the theoretical data of Griem to our experimental results.

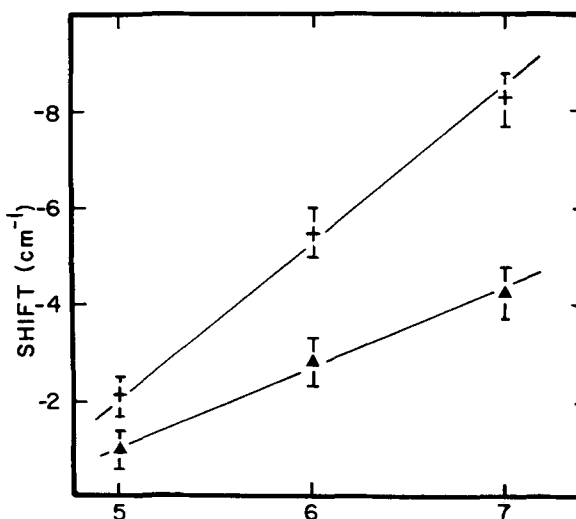


FIG. 8. Shift vs principal quantum number for $3^2P_{3/2} \rightarrow n^2D$ transitions, as determined from scans of the plasma emission (+) and absorption measurements (\blacktriangle) with 0.43 amagat of argon buffer.

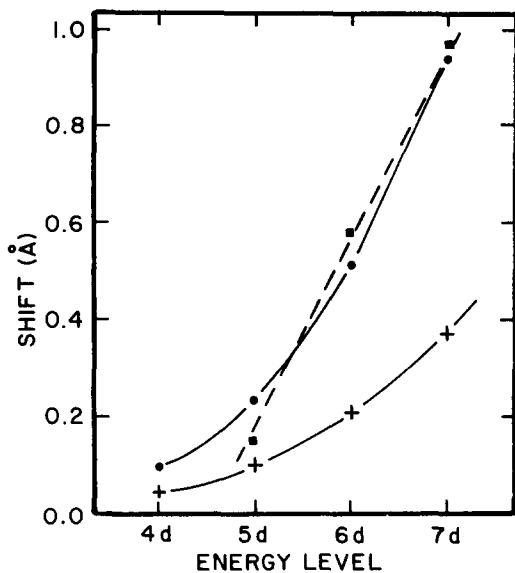


FIG. 9. Stark shift vs principal quantum number calculated by Griem for $T_e=10\,000\text{ K}$, $n_e=6.8\times 10^{14}\text{ cm}^{-3}$ (+), $T_e=900\text{ K}$, $n_e=6.8\times 10^{14}\text{ cm}^{-3}$ (•); and experimental points (■).

E. Electron density measurements from charge collection

An electric field applied across the interaction region defined by the laser beams can be used to extract charge produced in the excitation-ionization process. At the electron densities of this experiment, the Debye shielding length is less than the diameter of the reaction region; consequently, the electric field does not penetrate completely into the line charge and only a small portion of the charge is collected by the electrodes. Those electrons that are removed from the interaction volume cannot, of course, participate in the recombination process.

The application of a 100 V/cm electric field to the interaction volume reduces the integrated recombination fluorescence by approximately 20%. Equating this reduction to the measured charge collected at the electrodes, we find that the electron density of the laser-induced plasma is $3\times 10^{14}\text{ cm}^{-3}$.

The results obtained in this section are intended to be suggestive only and are included only because the electron densities obtained agree within reasonable expectations with the electron density measurements obtained from the line shift data and the Saha-Boltzmann plots.

TABLE I. Electron density measurements.

Electron density (cm^{-3})	Method
3.4×10^{14}	Saha-Boltzmann plot
4.1×10^{14}	Stark shift ($5d\rightarrow 3p$)
7.1×10^{14}	Stark shift ($6d\rightarrow 3p$)
7.0×10^{14}	Stark shift ($7d\rightarrow 3p$)
3.0×10^{14}	Charge extraction

IV. SUMMARY

The electron density in a laser-excited Na plasma at high buffer gas pressures has been measured in three different ways: (1) Saha-Boltzmann plots, (2) spectral line shifts due to electron collisions, and (3) charge extraction.

The results are summarized in Table I. The laser excitation and cell conditions are identical in each case. The Saha plots depend upon an absolute calibration of the detection system to determine the electron density and is reliable only to within a factor of 3. The electron temperature, however, depends only a relative calibration which is accurate to 10%. The electron density measurement from the charge extraction depends on some assumptions which appear to be reasonable but could not be independently verified.

Thus, despite the variation in the measured electron densities shown in Table I, we regard the different methods of obtaining the electron density as yielding satisfactory results. Both methods 1 and 2 are non-contact, nonperturbative methods. The spectral line shifts are, however, far easier to determine with good precision.

¹(a) T. B. Lucatorto and T. J. McIlrath, *Phys. Rev. Lett.* **37**, 428 (1976); (b) T. J. McIlrath and T. B. Lucatorto, *ibid.* **38**, 1390 (1977).

²R. M. Measures and P. G. Cardinal, *Phys. Rev. A* **23**, 804 (1981).

³G. H. Bearman and J. J. Levanthal, *Phys. Rev. Lett.* **41**, 1227 (1978).

⁴M. Allegrini, G. Alzetta, A. Kopystynska, L. Moi, and G. Orriols, *Opt. Commun.* **19**, 96 (1976).

⁵D. Krebs and L. D. Schearer, *J. Chem. Phys.* **75**, 3340 (1981).

⁶J. F. Kielkopf and R. B. Knollenburg, *Phys. Rev. A* **12**, 559 (1975).

⁷H. R. Griem, *Plasma Spectroscopy* (McGraw-Hill, New York, 1964).